THE JOURNAL OF PHYSICAL CHEMISTRY A

Article

Cite This: J. Phys. Chem. A 2019, 123, 4863−4872

pubs.acs.org/JPCA

Mechanism of Visible-Light Photooxidative Demethylation of Toluidine Blue O

José Robinson-Duggon,[†,‡] Nory Mariño-Ocampo,[†] Pablo Barrias,[§] Daniel Zúñiga-Núñez,[§] Germán Günther,[∥] Ana María Edwards,[†] Alexander Greer,[*,⊥,#] and Denis Fuentealba[*,†]

[†]Laboratorio de Química Biosupramolecular, Facultad de Química y de Farmacia, Pontificia Universidad Católica de Chile, Vicuña Mackenna 4860, Macul, Santiago, Chile

[‡]Departamento de Bioquímica, Facultad de Ciencias Naturales, Exactas y Tecnología, Universidad de Panamá, Panamá 0824, Panamá

[§]Laboratorio de Cinética y Fotoquímica, Facultad de Química y Biología, Universidad de Santiago de Chile, Alameda 3363, Estación Central, Santiago, Chile

[∥]Facultad de Ciencias Químicas y Farmacéuticas, Departamento de Química Orgánica y Fisicoquímica, Universidad de Chile, Casilla 233, Santiago, Chile

[⊥]Department of Chemistry, Brooklyn College, City University of New York, Brooklyn, New York 11210, United States

[#]Ph.D. Program in Chemistry, The Graduate Center of the City University of New York, 365 Fifth Avenue, New York, New York 10016, United States

S *Supporting Information*

ABSTRACT: Experiments and theoretical calculations by density functional theory (DFT) have been carried out to examine a self-sensitized type I photooxidation of toluidine blue O (TBO^+). This study attempts to build a connection between visible-light photolysis and demethylation processes of methylamine compounds, such as TBO^+. We show that controlled photoinduced mono- and double-demethylation of TBO^+ can be achieved. The kinetics for the appearance rate of the mono-demethylated TBO^+ and the double-demethylated TBO^+ were found to fit pseudo-first-order kinetics. DFT calculations have been used to examine the demethylation of TBO^+ and included *N,N*-dimethylaniline as a model compound for TBO^+. The results show an oxygen-dependent demethylation process. The mechanism for the sequential methyl loss is proposed to be due to $H^\bullet$ or e^-/H^+ transfer to $^3TBO^{+}*$ followed by a reaction of $TBO^{+\bullet}$ with O_2, yielding a *C*-peroxyTBO$^{+\bullet}$ intermediate. Instead of aminyl radical peroxyl formation, i.e., *N*-peroxyTBO$^{+\bullet}$, the C-centered peroxyTBO$^{+\bullet}$ is favored, that upon dimerization (Russell mechanism) leads to dissociation of formaldehyde from the methylamine site.

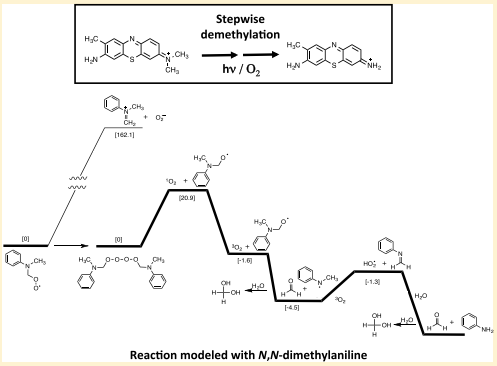

INTRODUCTION

Type I and type II photoreactions are oxygen-dependent and involve the initial formation of several reactive oxygen species (ROS) (Scheme 1). These type I and type II reactions include ROS such as ROO$^\bullet$, RO$^\bullet$, OH$^\bullet$, $^1O_2$, $HO_2^\bullet$, and $O_2^{\bullet-}$, and their formation depends on the concentration of sensitizer, the oxygen concentration, as well as the reactivity of substrate and/or solvent.[1−5]

The use of light to trigger a photooxidative demethylation is fundamentally interesting, but it is also potentially synthetically useful[6−8] and relates to the persistence of dyes against photodegradation[9,10] and may even represent photobiologically significant processes, although its mechanism remains poorly understood. Davidson et al. reported on the photooxidative demethylation for aryl amines in the 1970s.[11−13] Currently, photoredox catalysis routes to amination[14] or deprotection of tertiary amines[6] under mild visible-light irradiation are of much interest in synthetic chemistry. Moreover, photooxidative demethylation of DNA bases is also a topic of high interest.[7] There is presently a gap in knowledge on the mechanism of photosensitized O_2-dependent demethylation, including self-sensitized photodemethylation processes in aromatic (chromophoric) amines. We hypothesized that type I reactions in such systems would lead to peroxyl radical formation in the presence of oxygen. Peroxyl radicals can potentially dimerize to tetraoxides by the Russell reaction[15] and fragment to yield a number of products including carbonyls, alcohols, and singlet oxygen.[16] For this reason, we now address the topic for toluidine blue O (TBO^+), a known phenothiazinium photosensitizer and common dye stain in histology. Namely, we report on the results of a visible-light, self-sensitized TBO^+ demethylation process that was

Received: April 16, 2019
Revised: May 17, 2019
Published: May 22, 2019

DOI: 10.1021/acs.jpca.9b03588
J. Phys. Chem. A 2019, 123, 4863−4872

Scheme 1. Type I and Type II Photosensitized Oxidation Processes

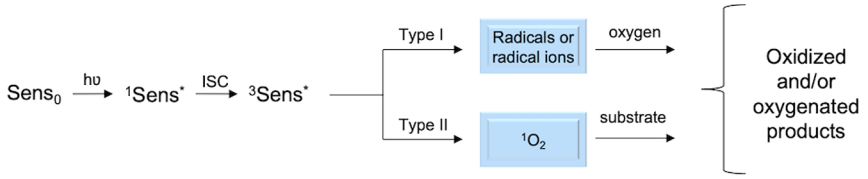

Scheme 2. Self-Sensitized TBO$^+$ Demethylation Induced by Visible-Light Irradiation

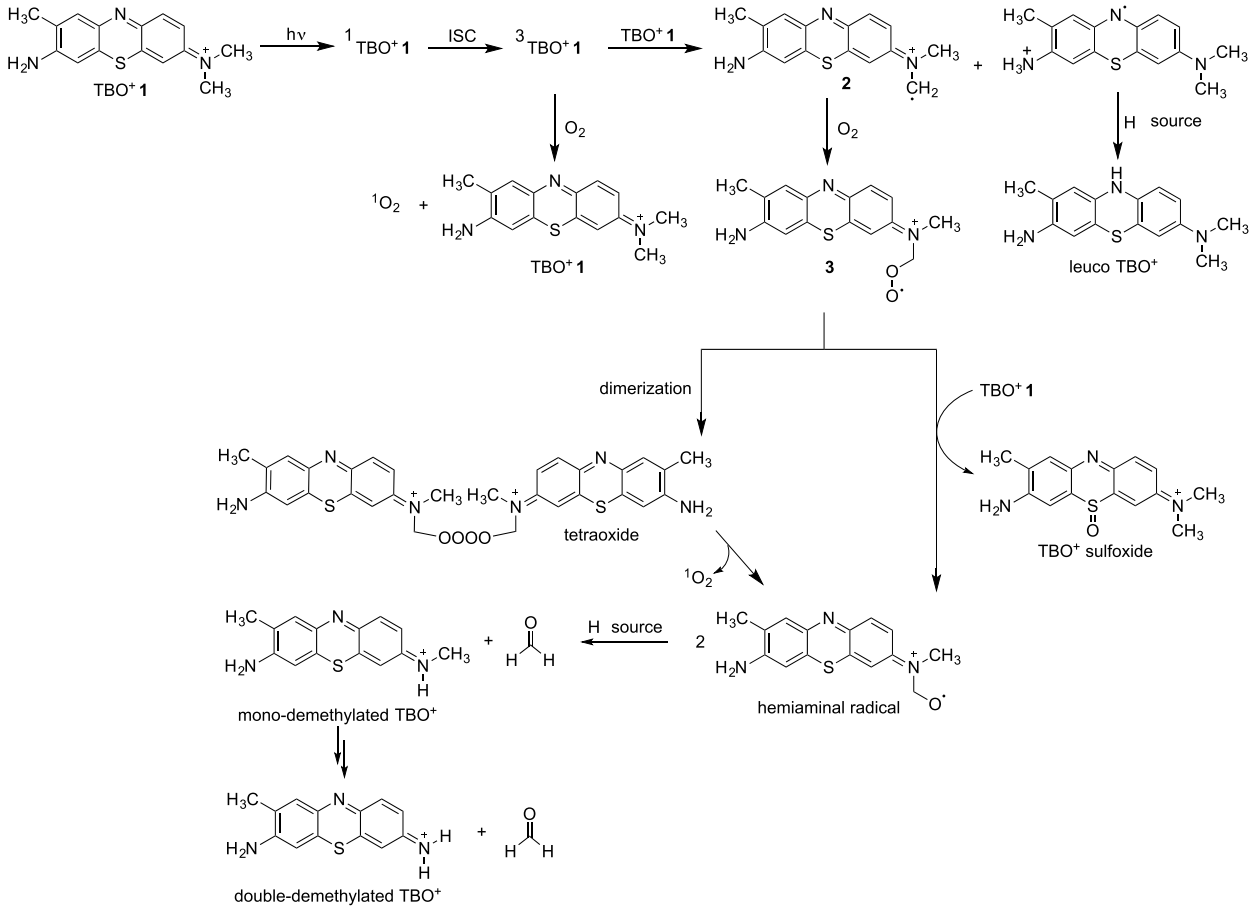

previously unappreciated. Moreover, the reaction was also considered more deeply with DFT calculations, where we modeled some of the type I TBO$^+$ demethylation processes with *N*,*N*-dimethylaniline (DMA). The experimental and theoretical data collected are consistent with the mechanism shown in Scheme 2, as will be discussed below.

RESULTS AND DISCUSSION

Photooxidative Demethylation of TBO$^+$. The visible-light irradiation of TBO$^+$ in the presence of oxygen in acetonitrile led to a change in the color of the solution from light blue to purple (inset in Figure 1), which is represented by a hypsochromic shift in the absorption maxima, as seen in Figure 1. This color-change behavior was not examined in a previous report.[17] Therefore, we have pursued the characterization of TBO$^+$ photoproducts to better understand the color change from blue to purple in aerated acetonitrile and buffer solutions.

Samples were irradiated at various time points and analyzed by UHPLC-MS/MS (Figures S1−S4 in the Supporting Information) to determine the photodegradation products. In particular, the masses of the mono-demethylated TBO$^+$ and double-demethylated TBO$^+$ were detected, according to the structures shown in Scheme 3. Interestingly, the mono-demethylated TBO$^+$ was the main product for up to 1 h of irradiation, followed by the appearance of the double-

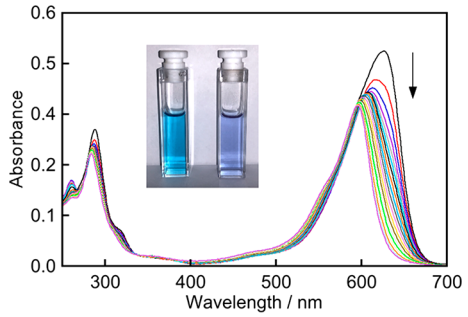

Figure 1. Absorption spectra for TBO$^+$ (12.5 μM) irradiated with visible light for 3 h in aerated-acetonitrile solution. The inset shows the color change from blue to purple after continued irradiation.

DOI: 10.1021/acs.jpca.9b03588
J. Phys. Chem. A 2019, 123, 4863−4872

Scheme 3. Structures of Compounds Assigned to Signals Detected by UHPLC-MS/MS from the Self-Sensitized Photooxidation TBO^+ under Visible-Light Irradiation in Aerated Acetonitrile

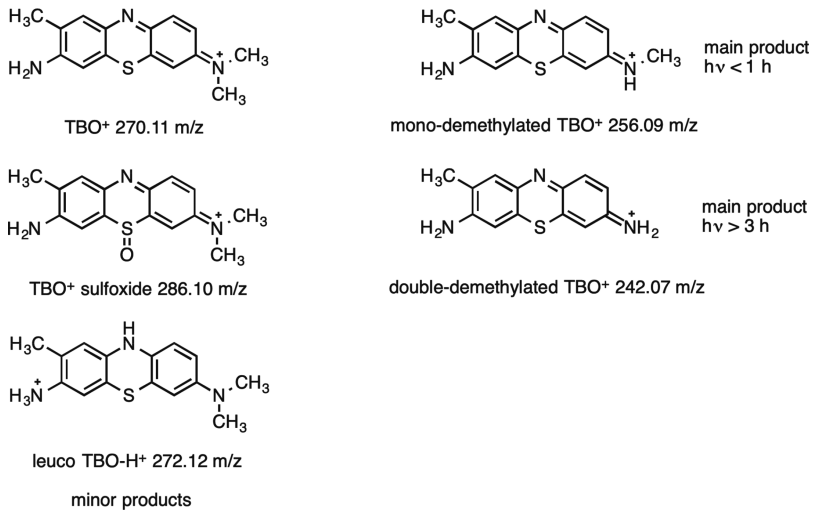

demethylated TBO^+. After 3 h of irradiation, the main product was the double-demethylated TBO^+, which was stable over time. As minor products, TBO^+ sulfoxide and protonated leuco-TBO^+ were also detected (Scheme 3).

Upon irradiation, a blue-shift in the maximum for TBO^+ was observed, as seen in Figure 1. The maximum for TBO^+ is 626 nm, and after 3 h of irradiation, it decreased to 595 nm, which we assigned to the double-demethylated product. This is based on quantum mechanical calculations using TD-DFT (B97D/6-311++G(d,p) in methanol, solvent simulation by the C-PCM model) to simulate the electronic absorption spectrum of the TBO^+, mono-demethylated TBO^+, and double-demethylated TBO^+, which showed a shift in the absorption maximum to shorter wavelengths as the methyl groups are lost (see Table S1 and Figures S5−S8 in the Supporting Information).

The kinetics for the disappearance of TBO^+ were followed past the maximum at 650 nm to avoid interference from the absorption of the photoproducts at shorter wavelengths (Figure 2). The kinetics were monoexponential and followed

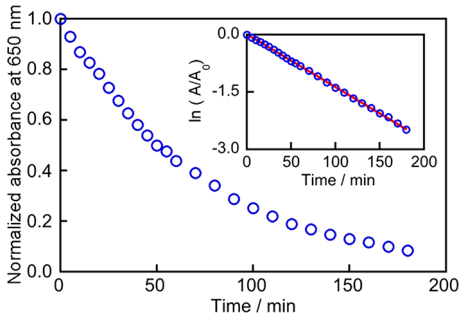

Figure 2. Kinetics for the photodegradation of TBO^+ in aerated-acetonitrile solution under visible-light irradiation. The inset shows the linear pseudo-first-order plot for the kinetics.

pseudo-first-order kinetics (inset in Figure 2). The interpretation of the pseudo-first-order kinetics is the conversion of TBO^+ to mono-demethylated TBO^+ compound.

When the TBO^+ solutions were purged with nitrogen (partial deoxygenation), a fast decomposition was observed followed by a slower process (see Figures S9 and S10). For this condition, the photoproducts detected were the same as those detected in the presence of higher amounts of oxygen (Figure S11), which points to a type I radical mechanism for the demethylation process. In fact, the participation of singlet oxygen was corroborated as minor on the basis of chemical trapping experiments in D_2O-enriched solutions (Figure S12). In phosphate buffer pH 7 (aerated solutions), we observed a marked photobleaching with no appreciable change in the color of the solution to the naked eye (see Figure S13). The photoproducts detected by UHPLC-MS/MS were the same as those detected in acetonitrile (see Figure S14), suggesting that photobiological applications of TBO^+ have an added caveat of forming mixtures of demethylated byproducts. In order to study the mechanism of methyl loss from TBO^+, including candidate methyl-small molecule byproducts, we carried out DFT calculations, which also enabled an assessment of regioselectivity of the demethylation mechanism.

DFT Calculations. Three main types of calculations were carried out: (1) the formation of a C-centered peroxy-TBO via a $TBO^{+\bullet}$ radical cation, (2) formation of a C-centered peroxy-DMA, and (3) demethylation paths of DMA as a model of TBO^+.

Computed Formation of Peroxy-Toluidine Blue. Our first aim was to determine the site on TBO^+ with the lowest hydrogen atom affinity (HAA) (Figure 3). The energy of H atom loss at the methylamine C−H (path A) is found to be lower compared to the amine N−H (path C) (397.7 compared to 407.7 kcal/mol, respectively). Figure S15 shows the HAA for the formation of radical cation **2**, as well as the formation of radical cations B−E and allylic diradical cations F−I, where we consider the oxygenation of the $N-CH_2^{\bullet}$ site to account for the experimentally observed mono- and double-demethylation of TBO^+. Path A is the lower energy path, wherein H atom loss is attributed to a self-photosensitized reaction. Our result builds on the work of Foote et al. that showed the tendency for H atom loss from electron poor sensitizers via the formation of radical cation or radical intermediates.[18,19] Our DFT results show that an addition of O_2 to TBO^+ is energetically favored at the methyl site rather than the amine site. The computed formation of peroxy $TBO^{+\bullet}$ **3** (path B) is favored over the peroxynitrogen $TBO^{+\bullet}$ **5** (path D), path B is exothermic and path D is endothermic. Structure **3** also has a longer C−O bond (1.47 Å) compared to the N−O bond in **5** (1.42 Å). In

DOI: 10.1021/acs.jpca.9b03588
J. Phys. Chem. A 2019, 123, 4863−4872

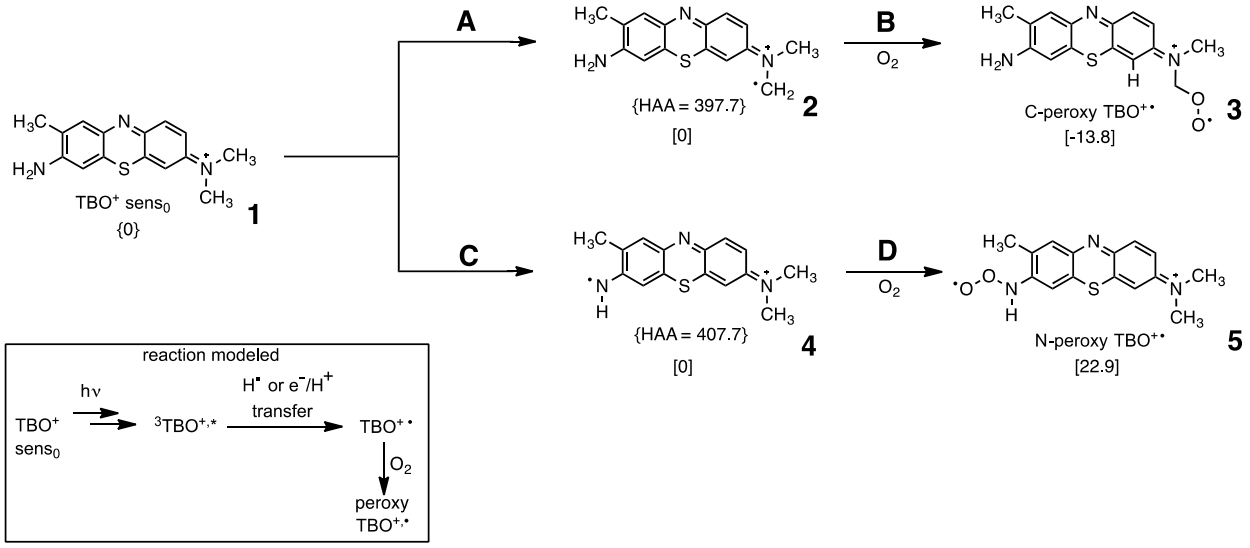

Figure 3. B3LYP/6-31G(d) calculated reactions for hydrogen atom loss from TBO^+ (**1**) to form the *C*-centered radical cation **2** and *N*-centered radical cation **4** and subsequent addition of molecular oxygen. The lower energy path is the conversion of **1** to **3**. Hydrogen atom affinity (HAA) values are shown in curly brackets, and the energies for the oxygenation of **2** and **4** are shown in square brackets. Gas phase energies are shown in kcal/mol.

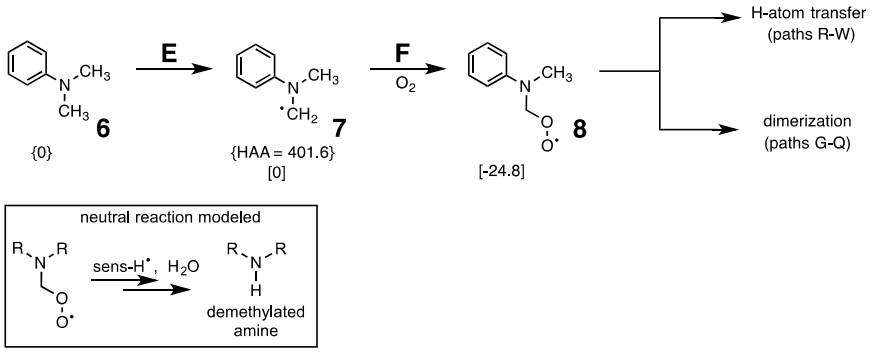

Figure 4. B3LYP/6-31G(d) calculated reactions for hydrogen atom loss from *N*,*N*-dimethylaniline (DMA) to form $DMA^•$ radical and subsequent addition of molecular oxygen to the C-centered radical **7**. Hydrogen atom affinity (HAA) values are shown in curly brackets, and the energy value for the oxygenation of **7** is shown in square brackets. Gas phase energies are shown in kcal/mol.

this vein, the formation of *C*-peroxy $TBO^{+•}$ **5** is reminiscent of oxygenation reactions of carbon radicals.[20] Formation of peroxyamines such as $R(H)NOO^•$ **5** is often associated with high-energy processes.[21]

Computed Formation of Peroxy N,N-Dimethylaniline. Our second aim used DFT calculations on *N*,*N*-dimethylaniline (DMA) as a model of a dimethylamine portion of TBO^+ to reduce the computational expense. Figure 4 (path E) shows H atom loss from the methylamine site via radical **7**, and path F shows the subsequent oxygenation to reach the peroxy-DMA radical **8**. The hydrogen atom affinities of the methylamine sites of TBO^+ (397.7 kcal/mol) and DMA (401.6 kcal/mol) are similar to each other to reach the $TBO^{•+}$ **2** and $PhCMe(CH_2^•)$ **7**, respectively.

Computed Demethylation of N,N-Dimethylaniline (DMA). Our third aim was to examine the demethylation on the basis of a dimerization of peroxyl radicals (Figure 5, paths G−Q). The dimerization of **8** is reminiscent of the Russell reaction of peroxy radicals in organic reactions and lipids.[22−24] The DFT calculations show that the energy for the decomposition of $PhN(Me)CH_2OO^•$ **8** is fairly low, 20 kcal/mol. Path G shows a dimerization of peroxyl radical $PhN(Me)CH_2OO^•$ **8** to reach the tetraoxide $PhN(Me)CH_2OOOOCH_2(Me)NPh$ **9**. Path H shows the decomposition of tetraoxide **9** into 2 mol of alkoxy radical $PhN(Me)CH_2O^•$ **10** and singlet oxygen ($^1O_2$). Calculating the conversion of $^1O_2$ to $^3O_2$ in path I would require multiconfigurational calculations,[25,26] and therefore, we used the known experimental value of 22.5 kcal/mol. Path J shows that alkoxy radical $PhN(Me)CH_2O^•$ **10** can decompose to formaldehyde (CH_2═O) and aminyl radical $Ph(Me)N^•$ **11**. Path J serves as a model reaction for *C*-peroxy$TBO^{+•}$ **3** that loses formaldehyde after formation of the hemiaminal (═$N^+(Me)CH_2O^•$ segment) from an initial oxygen atom transfer to TBO^+ **1** yielding the TBO^+ sulfoxide (Scheme 2). Formaldehyde can be hydrated to form formalin ($HO-CH_2OH$); since it is a well-known carbonyl hydration reaction,[27] it was deemed unnecessary to model.

Two subsequent paths can then lead to loss of the second methyl group. First, path L for the reaction of the aminyl radical $Ph(Me)N^•$ **11** with oxygen is endothermic by 3.2 kcal/mol, producing $HO_2^•$ and imine **12** that can release aniline and formaldehyde and subsequent hydration accounting for the loss of the methyl group. The hydration of imines and release of carbonyl compounds is a facile process due to the greater stability of the C═O bond compared to the C═N bond.[28] Second, paths M−P shown in Figure 6 can reach *N*-

DOI: 10.1021/acs.jpca.9b03588
J. Phys. Chem. A 2019, 123, 4863−4872

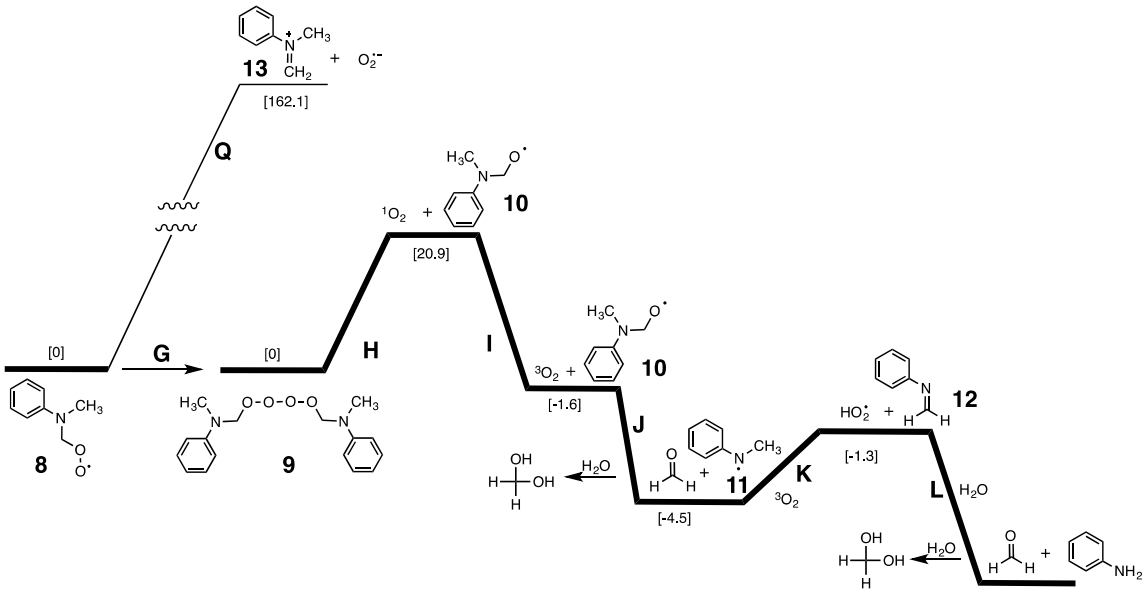

Figure 5. B3LYP/6-31G(d) calculated reactions for hydrogen atom loss from DMA to form DMA radical and subsequent dimerization, fragmentation, hydration, and electron transfer reactions. Aminyl radical **11** reacts to produce aniline in a direct double-demethylated DMA sequence. Gas phase energies are shown in kcal/mol.

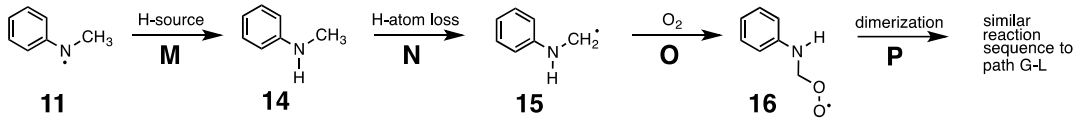

Figure 6. Reactions of aminyl radical **11**. Path M represents the formation of a mono-demethylation product **14**, as was seen experimentally with TBO^+. Further reaction of **14** includes H atom loss, peroxidation, dimerization, and fragmentation steps to account for a net double-demethylated DMA pathway.

methylaniline **14**, and the corresponding radical **15** and peroxy radical **15**, for dimerization to tetraoxide and decomposition in a manner similar to paths G–J. The data suggest that $PhN(Me)CH_2OO^\bullet$ **8** decomposition is a fairly low energy process. An electron transfer reaction (path Q) to a peroxy radical to iminium ion $Ph(Me)N^+{=}CH_2$ and superoxide $O_2^{\bullet-}$ was also sought but has been ruled out, since it is high in energy (162 kcal/mol).

The hydroperoxyl radical $PhN(Me)CH_2OO^\bullet$ **8** can scavenge a H atom to reach the neutral hydroperoxide $PhN(Me)CH_2OOH$ **17**. Compound **8** has a longer C–O bond (1.51 Å) compared to **17** (1.45 Å). On the other hand, the O–O bond of **8** (1.32 Å) is shorter compared to **17** (1.46 Å).

Alternative Computed Demethylation Paths. Next, we show that alternative demethylation paths are high in energy (paths R–Z, Figures 7 and 8). The calculations show that the energies for $PhN(Me)CH_2OOH$ **17** decomposition ranged from 34 to 74 kcal/mol. The hydroperoxide **17** N–CH_2 bond is slightly shorter (1.42 Å) than the H_2C–O bond (1.45 Å). Path R shows the activation barrier of 34.5 kcal/mol via **TS17/18** to reach *N*-methylaniline **18** and carbonyl oxide. We also find the decomposition of **17** to be endothermic by 33.7 kcal/mol. Path S shows an activation barrier of 57.5 kcal/mol via **TS17/19** to reach amide **19** and water. Other paths (paths T–W) are even higher in energy, including path T (O–O homolysis to alkoxy radical **10** and $^\bullet OH$), path U (N–CH_3 homolysis to aminyl radical **20** and $^\bullet CH_3$), and path V (N–CH_2 homolysis to aminyl radical **11** and $^\bullet CH_2OOH$ **21**). A saddle point which connects **17**, imine **12**, and CH_3OOH has been located (path W), but this methyl "walk" rearrangement is very high in energy (74.3 kcal/mol). Constrained calculations were applied to obtain rough estimations of bond dissociation energies of the O–O bond in path T, the N–C(1) bond in path U, and the N–C(2) bond in path V.

Figure 8 shows path X for protonation of hydroperoxide **17**, which occurs at the nitrogen atom with a proton affinity of 223.8 kcal/mol. Hydroperoxide ion **21** has a N–CH_2 bond that is longer (1.55 Å) and weaker than the H_2C–O bond (1.37 Å). However, bond separation scans (carried 1.5 Å beyond their normal bond lengths) show these paths to be high in energy. Namely, path Y shows the hydroperoxide ion **21** cleaves *N*-methylaniline and protonated carbonyl oxide (H_2C^+OOH) with a bond separation energy of 39.5 kcal/mol, and path Z is a H_2C–O homolysis to benzenaminium radical cation **23** and $HOO^\bullet$ with a bond separation energy of 72.8 kcal/mol.

Detection of Formaldehyde as a Byproduct. The above DFT results lead us to predict the formation of formaldehyde, which was then tested experimentally. Indeed, we found that the photooxidative demethylation of TBO^+ identified above involving the formation of peroxyl radicals leads to the loss of the methyl groups as formaldehyde molecules. Experimentally, we trapped formaldehyde from the self-sensitized TBO^+ photooxidation reaction by formaldehyde's derivatization with 2,4-dinitrophenylhydrazine (DNPH) and HPLC chromatographic separation and quantification (Figure 9). It should be mentioned that formaldehyde exists primarily as formalin (hydrated formaldehyde) in the presence of water. After 1 h of irradiation, we detected the formation of ~0.5 equiv of formaldehyde with respect to the concentration

DOI: 10.1021/acs.jpca.9b03588
J. Phys. Chem. A 2019, 123, 4863–4872

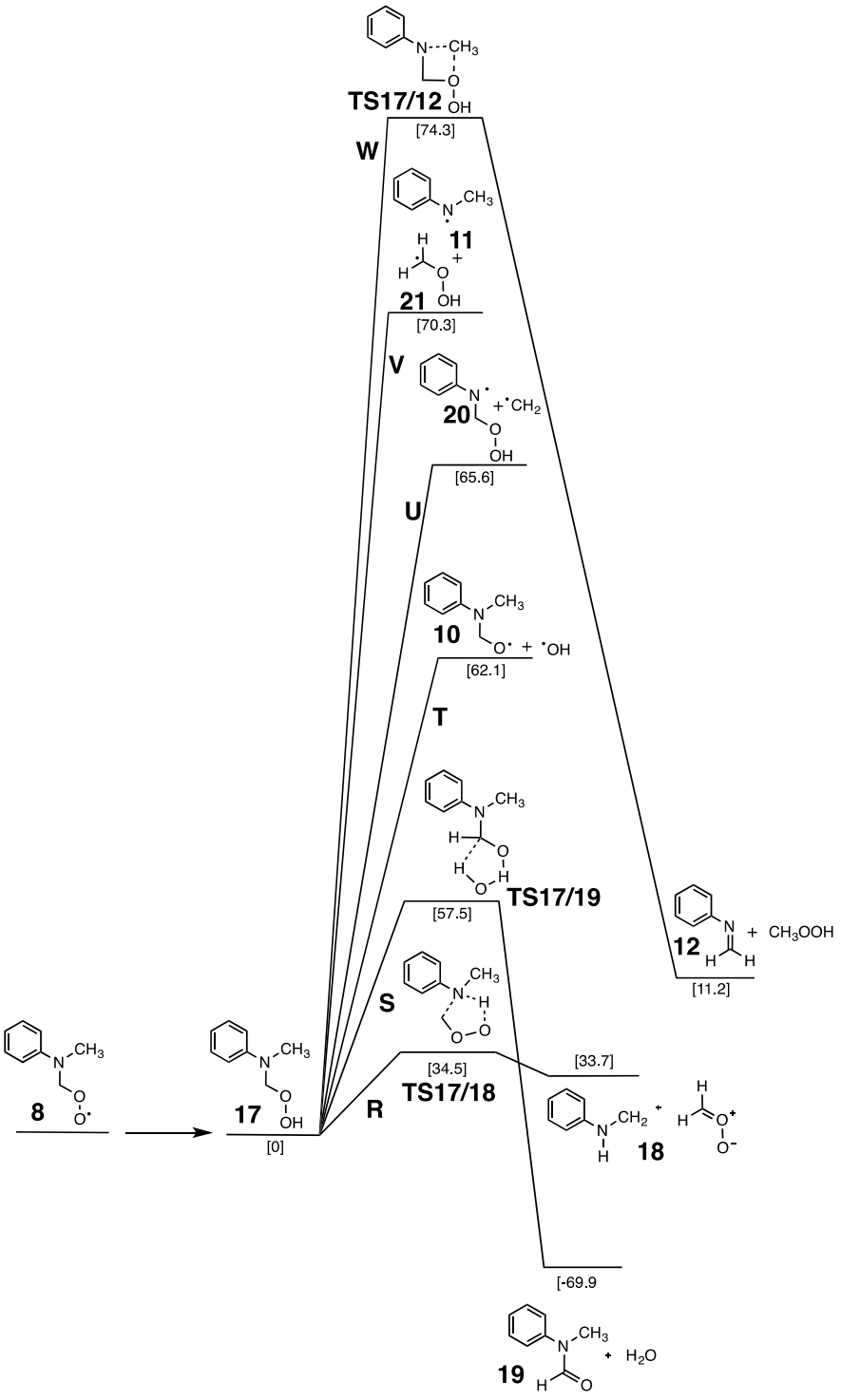

Figure 7. B3LYP/6-31G(d) calculated reactions for the conversion of peroxyl radical **8** to hydroperoxide **17** and fragmentation reactions. Gas phase energies are shown in kcal/mol.

of TBO^+, which was quantified by the use of a standard. After 3 h of irradiation, the amount of formaldehyde that could be detected was minor, suggesting formaldehyde does not accumulate and keeps reacting (see Figure S16 in the Supporting Information).

Proposed Mechanism. To determine the factors that underlie TBO^+ demethylation photochemistry in the presence of O_2, three mechanistic facets were studied. One derives from the reaction of C-centered radical with O_2 via peroxyl radical intermediates that cleave apart, the second from formaldehyde release, and the last is the viability of the carbonyl oxide intermediates.

(1) The calculations determined the lowest-energy demethylation path that we based on a dimerization of peroxyl radicals leading to an alkoxy radical that releases formaldehyde. Aminyl radical reaction with O_2 produces imine to release a second formaldehyde molecule. The protonation of aminyl radicals to aminium radical cations ($R_2NH^{+\bullet}$) is also shown to

DOI: 10.1021/acs.jpca.9b03588
J. Phys. Chem. A 2019, 123, 4863−4872

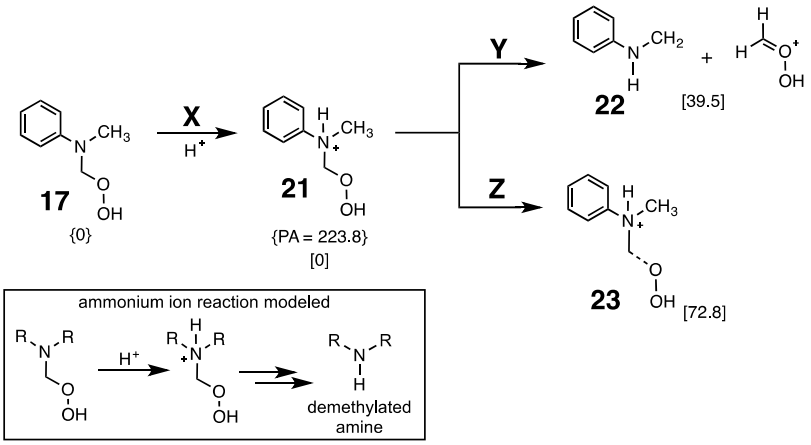

Figure 8. B3LYP/6-31G(d) calculated reactions for the conversion of hydroperoxide **17** to protonated hydroperoxide **18** and subsequent fragmentation reactions. Proton affinity (PA) values are shown in curly brackets, and the energy for the oxygenation of **7** is shown in square brackets. Gas phase energies are shown in kcal/mol.

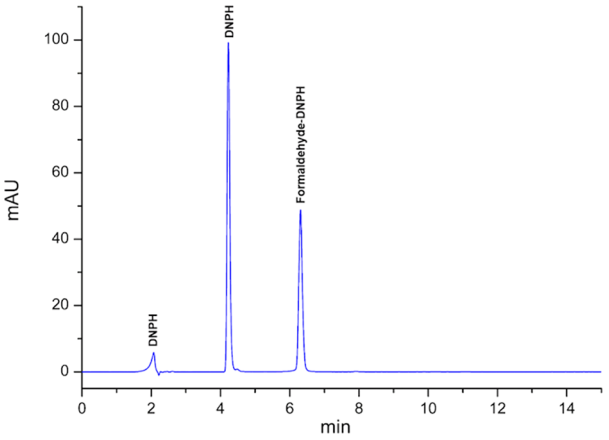

Figure 9. HPLC detection of the formaldehyde-DNPH derivative at 360 nm using acetonitrile:water (60:40) as the mobile phase on a C18 reverse phase column. The samples were irradiated for 1 h under visible light.

react only slowly with O_2, on the basis of unaffected absorption signals in the presence of O_2.[29] The calculations predict the existence of C−OO $TBO^{+\bullet}$ **3** but not the N−OO $TBO^{+\bullet}$ **5** with the former having greater stability. In paths A and B, as well as paths E and F, hydrogen-atom loss leads to addition of O_2 and the peroxy intermediate.

(2) We propose that the photooxidative demethylation of TBO^+ mainly involves a Russell reaction with the dimerization of the peroxy intermediate to form a tetraoxide. We found a decomposition of tetraoxide **9** by Russell-like intermediates (paths H−J). Paths G−L account for the double demethylation process through release of formaldehyde/formalin. The results are understandable in terms of the formation of aminyl radical **11** and paths M−P such as peroxy radical **16** formation that explain the sequential demethylation and the experimental formation of mono-demethylated TBO^+.

(3) The formation of a carbonyl oxide is not likely due to a higher energy path (path R) compared to the decomposition of the tetraoxide (path H). Peroxidation can lead to methyl loss but not by eliminating carbonyl oxide. It can also be noted that the high-energy path to release of superoxide (path Q) was not found. Furthermore, it should be noted that the photolysis of TBO^+ leads to $^1O_2$ that can interact with the nitrogen sites. Nitrogen-containing groups can interact with $^1O_2$ by a physical quenching process, which has been detected with amines, nitrosamines, hydrazines, and diazo compounds.[30,31] The k_T value (total quenching rate constant which is the sum of physical and chemical quenching rate constants) of quinoline is $<1 \times 10^9$ M^{-1} s^{-1},[32] that of dimethylanilines is 1×10^9 M^{-1} s^{-1},[33] and that of 8-hydroxyquinoline is 1.1×10^8 M^{-1} s^{-1}.[34] This physical quenching is often by a charge-transfer process; however, this process was not modeled.

The DFT calculations support the oxidation products detected by mass spectrometry. The theoretical work has also shown amine hydrogens to be labile to proton loss when compared with the available experimental data as compared with hydrogen atom loss.

In summary, as described above, a visible-light photooxidative process that demethylates TBO^+ was discovered and it is an oxygen-dependent process. DFT calculations provided insight into the mechanism of demethylation. We found that the C-centered radical **2** is more stable than aminyl radical **4** by 10.0 kcal/mol. The computations also predicted an exothermic addition of O_2 to the C-centered radical of TBO^+ and DMA. The computations did not predict the addition of O_2 to the aminyl radical undoubtedly because of the endothermicity of the reaction. Indeed, we found that the peroxy radical **3** is more stable compared to the peroxyamine radical **5** by 32.9 kcal/mol. Masses were obtained for stable products such as sulfoxide and rearranged products, but masses of the proposed peroxide and radical intermediates were not obtained, as they are short-lived species. In this TBO^+ system, future experiments could include low-temperature mass spectrometry of short-lived species, which aided in characterizing unstable episulfoxide, oxaphosphetane, and endoperoxide intermediates.[35−37]

■ CONCLUSIONS

Our work contributes to the fundamental understanding of aromatic amine demethylation induced by visible light, which is relevant to photoredox catalysis, degradation, synthesis, and photobiological processes. The demethylation pathways uncovered herein are relevant to the widespread use of TBO^+ and related molecules as dyes, where a demethylation process can modify the interpretation of results due to

DOI: 10.1021/acs.jpca.9b03588
J. Phys. Chem. A 2019, 123, 4863−4872

exposure to formaldehyde/formalin. In this context, shifts in absorption maxima under visible-light irradiation should be examined carefully.

EXPERIMENTAL SECTION

Chemicals. Toluidine blue O was obtained from Sigma and purified using flash chromatography on silica gel with ethanol:HCl (99:1) as eluent. 9,10-Anthracene-bis-(methylene)dimalonic acid (ABMA) was obtained from Sigma and used without further purification. Solvents such as ethanol, methanol, acetonitrile, and HCl (37% w/w) were of the highest purity available and were purchased from Merck. Deionized water was obtained using a Millipore water purification system. Stock solution of TBO^+ in acetonitrile was prepared fresh, and aliquots were diluted to an absorbance of 0.5 at 626 nm for the irradiation experiments.

Absorption Measurements and Irradiation Setup. Absorption spectra were collected with a HP8453 UV−visible spectrophotometer using a 1 cm path length cell. Samples were irradiated using a tungsten filament lamp from a commercial slide projector, filtered with a 400 nm cutoff filter, and focused onto the cell using a focusing lens (PTI). The light intensity was 195 W/m^2 (Delta OHM photoradiometer model HD 2302.0), and the lamp had an emission spectrum between 350 and 850 nm with a peak of intensity at 550 nm (Luzchem spectroradiometer model SPR-01-235-850 nm).

Oxidation Product Analysis by UHPLC-MS/MS. Samples were measured using an Ultra-High Performance Liquid Chromatography (UHPLC) Ultimate 3000 RSLC system coupled to a Linear Ion Trap Mass Spectrometer LTQ XL (Thermo scientific). An HP InertsilODS-4 (3 μm, 2.1 × 100 mm^2, GL Sciences) column maintained at 25 °C was used as the stationary phase, and isocratic elution with a solution of methanol 100% containing formic acid 0.1% at a flux of 0.2 mL/min was employed as the mobile phase. The mass detection was carried out through electrospray ionization (ESI), and the spray voltage was set at 3 kV at 350 °C. Detection was performed in full scan mode in the 100−1000 m/z range in positive mode. The MS^2 results were performed using He as collision gas for collision-induced dissociation (CID) with a normalized collision energy of 35 units and detection of fragments in full scan mode for all samples.

Computational Methods. Calculations were carried out with the Gaussian 09 program package.[38] Structures were optimized with B3LYP/6-31G(d) calculations and visualized with Gaussview 5.0.[39] Structures were optimized to minima or maxima. Transition structures have been verified as transition states by frequency calculations.[40] In some cases, calculations were carried out by scanning of bond rotations and bond dissociations by constraining compound geometries. Selectivity of H atom loss from TBO^+ was examined at both the southeastern methyl and the northeastern methyl, but it was found to differ only trivially so this data is not included in the Results and Discussion section. Similarly, the selectivity of H atom loss from TBO^+ was examined from the western and southwestern amine hydrogens and was also not found to differ significantly. The hydrogen loss from excited states of TBO^+ was not computed. Due to size constraints in the DFT calculations, *N*,*N*-dimethylaniline (DMA) was used as a model of TBO^+. Gas phase energetics are reported in kcal/mol and have included thermal corrections for enthalpy.

Calculation of Electronic Absorption Spectra. The quantum mechanical calculations were performed using DFT with the Gaussian 09 package.[38] Stationary points on the potential energy surface were obtained using the B3LYP hybrid density functional.[41,42] A full molecular geometry optimization of the ground state of TBO^+ and demethylated TBO^+ was performed in acetonitrile using the 6-311++G (d,p) basis set for all atoms.[43,44] The converged wave functions were verified by analytical computations of harmonic vibrational frequencies. Once the optimized geometry was obtained, the calculation of the excited electronic states was carried out by the time-dependent TD-DFT methodology to obtain the UV−visible and emission spectra for each molecular system.[45,46] With the aim of finding the best functional that predicts the experimental result, we performed a calibration study of the functional. To do that, we calculated the electronic absorption spectrum with different functionals, such as B97D,[47] PBE,[48,49] BKM,[50] M06,[51] B3LYP, CAM-B3LYP,[52] HSEH1PBE, wB97, and wB97x.[50] That functional predicting the lower experimental deviation was chosen. The UV−visible spectra were obtained by singlet−singlet vertical transitions of Franck−Condon type using 30 excited states. Spectra were calculated in the solution phase (solvent acetonitrile). The modeling of the solvent was carried out using the conductor-like polarizable continuum model (C-PCM) with the standard parameters for each solvent.[53]

HPLC Detection of Formaldehyde. Formaldehyde was derivatized with DNPH from a commercial kit according to the manufacturer. Later, 20 μL was injected in an HPLC using acetonitrile:water (60:40) (v:v) as a mobile phase, a flow of 1 mL min^{-1}, a C18 reverse phase column, and a detection wavelength of 360 nm. The temperature of the column was 40 °C.[54] The concentration of formaldehyde was estimated by interpolating between the integrated HPLC peaks of known standards (2 and 10 μM).

ASSOCIATED CONTENT

Supporting Information

The Supporting Information is available free of charge on the ACS Publications website at DOI: 10.1021/acs.jpca.9b03588.

Mass spectra for TBO^+ photoproducts, simulations of the absorption spectra, photooxidation in buffer, and HPLC detection of formaldehyde (PDF)

AUTHOR INFORMATION

Corresponding Authors

*E-mail: dlfuente@uc.cl.

*E-mail: agreer@brooklyn.cuny.edu.

ORCID

Pablo Barrias: 0000-0003-4072-4436

Alexander Greer: 0000-0003-4444-9099

Denis Fuentealba: 0000-0003-4798-7204

Notes

The authors declare no competing financial interest.

ACKNOWLEDGMENTS

A.G. acknowledges support from the National Science Foundation (CHE-1464975 and CHE-1856765). D.F. thanks CONICYT for the financial support through their FONDECYT research program (Grant No. 1160443) and CONICYT FONDEQUIP/UHPLC MS/MS EQM 120065 for mass spectrometry analysis. J.R.-D. thanks CONICYT-PCHA/Doctorado Nacional/2015-21150894. P.B. thanks CONI-

DOI: 10.1021/acs.jpca.9b03588
J. Phys. Chem. A 2019, 123, 4863−4872

CYT-PCHA/Doctorado Nacional/2016-21160605. D.Z.-N. thanks CONICYT-PCHA/Doctorado Nacional/2015-21151163.

REFERENCES

(1) Foote, C. S. Definition of Type-I and Type-II Photosensitized Oxidation. *Photochem. Photobiol.* **1991**, *54*, 659−659.

(2) Greer, A. Christopher Foote's Discovery of the Role of Singlet Oxygen [$^1O_2$ ($^1\Delta_g$)] in Photosensitized Oxidation Reactions. *Acc. Chem. Res.* **2006**, *39*, 797−804.

(3) Ghogare, A. A.; Greer, A. Using Singlet Oxygen to Synthesize Natural Products and Drugs. *Chem. Rev.* **2016**, *116*, 9994−10034.

(4) Sauvaigo, S.; Douki, T.; Odin, F.; Caillat, S.; Ravanat, J. L.; Cadet, J. Analysis of Fluoroquinolone-Mediated Photosensitization of 2′-Deoxyguanosine, Calf Thymus and Cellular DNA: Determination of Type-I, Type-II and Triplet−Triplet Energy Transfer Mechanism Contribution. *Photochem. Photobiol.* **2001**, *73*, 230−237.

(5) Davies, M. Free Radicals, Oxidants and Protein Damage. *Aust. Biochem.* **2012**, *43*, 8−12.

(6) Rueping, M.; Vila, C.; Szadkowska, A.; Koenigs, R. M.; Fronert, J. Photoredox Catalysis as an Efficient Tool for the Aerobic Oxidation of Amines and Alcohols: Bioinspired Demethylations and Condensations. *ACS Catal.* **2012**, *2*, 2810−2815.

(7) Xie, L. J.; Wang, R. L.; Wang, D.; Liu, L.; Cheng, L. Visible-light-mediated oxidative demethylation of *N*-6-methyl adenines. *Chem. Commun.* **2017**, *53*, 10734−10737.

(8) Rao, K. V. S.; Srinivas, B.; Boule, P.; Subrahmanyam, M. A Comparative and Mechanistic Study on Regioselective Photooxidative Demethylation of *N*-heterocyclics Using TiO_2 and Molecular Oxygen. *J. Chem. Technol. Biotechnol.* **2002**, *77*, 568−575.

(9) Zhang, T. Y.; Oyama, T.; Aoshima, A.; Hidaka, H.; Zhao, J. C.; Serpone, N. Photooxidative *N*-demethylation of Methylene Blue in Aqueous TiO_2 Dispersions Under UV Irradiation. *J. Photochem. Photobiol., A* **2001**, *140*, 163−172.

(10) Chen, C. C.; Fan, H. J.; Jang, C. Y.; Jan, J. L.; Lin, H. D.; Lu, C. S. Photooxidative *N*-demethylation of Crystal Violet Dye in Aqueous Nano-TiO_2 Dispersions Under Visible Light Irradiation. *J. Photochem. Photobiol., A* **2006**, *184*, 147−154.

(11) Bartholomew, R. F.; Davidson, R. S. The Photosensitised Oxidation of Amines. Part II. The Use of Dyes as Photosensitisers: Evidence That Singlet Oxygen is Not Involved. *J. Chem. Soc. C* **1971**, 2347−2351.

(12) Bartholomew, R. F.; Davidson, R. S. The Photosensitised Oxidation of Amines. Part I. The Use of Benzophenone as a Sensitiser. *J. Chem. Soc. C* **1971**, 2342−2346.

(13) Davidson, R. S.; Trethewey, K. R. Photosensitized Oxidation of Amines - Mechanism of Oxidation of Triethylamine. *J. Chem. Soc., Perkin Trans. 2* **1977**, 173−178.

(14) Wei, W.; Wang, L. L.; Bao, P. L.; Shao, Y.; Yue, H. L.; Yang, D. S.; Yang, X. B.; Zhao, X. H.; Wang, H. Metal-Free C(sp(2))-H/N-H Cross-Dehydrogenative Coupling of Quinoxalinones with Aliphatic Amines Under Visible-Light Photoredox Catalysis. *Org. Lett.* **2018**, *20*, 7125−7130.

(15) Russell, G. A. Deuterium-isotope Effects in the Autoxidation of Aralkyl Hydrocarbons. Mechanism of the Interaction of Peroxy Radicals. *J. Am. Chem. Soc.* **1957**, *79*, 3871−3877.

(16) Mano, C. M.; Prado, F. M.; Massari, J.; Ronsein, G. E.; Martinez, G. R.; Miyamoto, S.; Cadet, J.; Sies, H.; Medeiros, M. H. G.; Bechara, E. J. H.; Di Mascio, P. Excited Singlet Molecular O_2 ($^1\Delta_g$) is Generated Enzymatically from Excited Carbonyls in the Dark. *Sci. Rep.* **2015**, *4*, No. 5938.

(17) Robinson-Duggon, J.; Pérez-Mora, F.; Valverde-Vásquez, L.; Cortés-Arriagada, D.; De la Fuente, J. R.; Günther, G.; Fuentealba, D. Supramolecular Reversible On−Off Switch for Singlet Oxygen Using Cucurbit[*n*]uril Inclusion Complexes. *J. Phys. Chem. C* **2017**, *121*, 21782−21789.

(18) Foote, C. S. Dicyanoanthracene Sensitized Photo-Oxygenation of Olefins: Electron-Transfer and Singlet Oxygen Mechanisms. *Tetrahedron* **1985**, *41*, 2221−2227.

(19) Silverman, S. K.; Foote, C. S. Singlet Oxygen and Electron-Transfer Mechanisms in the Dicyanoanthracene-Sensitized Photooxidation of 2,3-Diphenyl-1,4-Dioxene. *J. Am. Chem. Soc.* **1991**, *113*, 7672−7675.

(20) Yin, H. Y.; Xu, L. B.; Porter, N. A. Free Radical Lipid Peroxidation: Mechanisms and Analysis. *Chem. Rev.* **2011**, *111*, 5944−5972.

(21) Ghogare, A. A.; Debaz, C. J.; Oliveira, M. S.; Abramova, I.; Mohapatra, P. P.; Kwon, K.; Greer, E. M.; Prado, F. M.; Valerio, H. P.; Di Mascio, P.; Greer, A. Experimental and DFT Computational Insight Into Nitrosamine Photochemistry - Oxygen Matters. *J. Phys. Chem. A* **2017**, *121*, 5954−5966.

(22) Miyamoto, S.; Martinez, G. R.; Rettori, D.; Augusto, O.; Medeiros, M. H. G.; Di Mascio, P. Linoleic Acid Hydroperoxide Reacts With Hypochlorous Acid, Generating Peroxyl Radical Intermediates and Singlet Molecular Oxygen. *Proc. Natl. Acad. Sci. U. S. A.* **2006**, *103*, 293−298.

(23) Miyamoto, S.; Martinez, G. R.; Medeiros, M. H. G.; Di Mascio, P. Singlet Molecular Oxygen Generated by Biological Hydroperoxides. *J. Photochem. Photobiol., B* **2014**, *139*, 24−33.

(24) Di Mascio, P.; Martinez, G. R.; Miyamoto, S.; Ronsein, G. E.; Medeiros, M. H. G.; Cadet, J. Singlet Molecular Oxygen Reactions with Nucleic Acids, Lipids, and Proteins. *Chem. Rev.* **2019**, *119*, 2043−2086.

(25) Garavelli, M.; Bernardi, F.; Olivucci, M.; Robb, M. A. DFT Study of the Reactions Between Singlet Oxygen and a Carotenoid Model. *J. Am. Chem. Soc.* **1998**, *120*, 10210−10222.

(26) Singleton, D. A.; Hang, C.; Szymanski, M. J.; Meyer, M. P.; Leach, A. G.; Kuwata, K. T.; Chen, J. S.; Greer, A.; Foote, C. S.; Houk, K. Mechanism of Ene Reactions of Singlet Oxygen. A Two-Step No-Intermediate Mechanism. *J. Am. Chem. Soc.* **2003**, *125*, 1319−1328.

(27) Rayne, S.; Forest, K. A High-Level Theoretical Study Into the Atmospheric Phase Hydration, Bond Dissociation Enthalpies and Acidity of Aldehydes. *J. Phys. Org. Chem.* **2016**, *29*, 336−345.

(28) Ciaccia, M.; Di Stefano, S. Mechanisms of Imine Exchange Reactions in Organic Solvents. *Org. Biomol. Chem.* **2015**, *13*, 646−654.

(29) Chow, Y. L. Nitrosamine Photochemistry. Reactions of Aminium Radicals. *Acc. Chem. Res.* **1973**, *6*, 354−360.

(30) Clennan, E. L.; Noe, L.; Szneler, E.; Wen, T. Hydrazines: New Charge-Transfer Physical Quenchers of Singlet Oxygen. *J. Am. Chem. Soc.* **1990**, *112*, 5080−5085.

(31) Wilkinson, F.; Helman, W. P.; Ross, A. B. Rate Constants for the Decay and Reactions of the Lowest Electronically Excited Singlet State of Molecular Oxygen in Solution - an Expanded and Revised Compilation. *J. Phys. Chem. Ref. Data* **1995**, *24*, 663−1021.

(32) Dalle, J. P.; Magous, R.; Mousseron-Canet, M. Inhibition De L'Oxygene Singulet. *Photochem. Photobiol.* **1972**, *15*, 411−419.

(33) Saito, I.; Matsuura, T.; Inoue, K. Formation of Superoxide Ion Via One-Electron Transfer from Electron-Donors to Singlet Oxygen. *J. Am. Chem. Soc.* **1983**, *105*, 3200−3206.

(34) Larson, R. A.; Marley, K. A. Quenching of Singlet Oxygen by Alkaloids and Related Nitrogen Heterocycles. *Phytochemistry* **1984**, *23*, 2351−2354.

(35) Sheu, C.; Foote, C. S. Endoperoxide Formation in a Guanosine Derivative. *J. Am. Chem. Soc.* **1993**, *115*, 10446−10447.

(36) Wang, C.-H.; Huang, M.-W.; Lee, C.-Y.; Chei, H.-L.; Huang, J.-P.; Shiea, J. Detection of a Thermally Unstable Intermediate in the Wittig Reaction Using Low-Temperature Liquid Secondary Ion and Atmospheric Pressure Ionization Mass Spectrometry. *J. Am. Soc. Mass Spectrom.* **1998**, *9*, 1168−1174.

(37) Greer, A.; Conklin, K. A.; Faull, K.; Houk, K. N.; Foote, C. S. Low-Temperature FAB Mass and NMR Spectroscopic Identification of Unstable Episulfoxides. *J. Org. Chem.* **1999**, *64*, 1432−1433.

DOI: 10.1021/acs.jpca.9b03588
J. Phys. Chem. A 2019, 123, 4863−4872

(38) Frisch, M. J.; Trucks, G. W.; Schlegel, H. B.; Scuseria, G. E.; Robb, M. A.; Cheeseman, J. R.; Scalmani, G.; Barone, V.; Mennucci, B.; Petersson, G. A.; et al. *Gaussian 09*, revision E.01; Wallingford, CT, 2009.
(39) Dennington, R.; Keith, T.; Millam, J. *Gaussview*; Semichem Inc.: Shawnee Mission, KS, 2009.
(40) Jensen, F. *Introduction to Computational Chemistry*, 2nd ed.; Wiley: Chichester, U.K., 2007.
(41) Becke, A. D. Density-Functional Thermochemistry. III. The Role of Exact Exchange. *J. Chem. Phys.* **1993**, *98*, 5648−5652.
(42) Lee, C.; Yang, W.; Parr, R. G. Development of the Colle-Salvetti Correlation-Energy Formula Into a Functional of the Electron Density. *Phys. Rev. B: Condens. Matter Mater. Phys.* **1988**, *37*, 785−789.
(43) Petersson, G. A.; Al-Laham, M. A. A Complete Basis Set Model Chemistry. II. Open-Shell Systems and the Total Energies of the First-Row Atoms. *J. Chem. Phys.* **1991**, *94*, 6081−6090.
(44) Petersson, G. A.; Bennett, A.; Tensfeldt, T. G.; Al-Laham, M. A.; Shirley, W. A.; Mantzaris, J. A Complete Basis Set Model Chemistry. I. The Total Energies of Closed-Shell Atoms and Hydrides of the First-Row Elements. *J. Chem. Phys.* **1988**, *89*, 2193−2218.
(45) Stratmann, R. E.; Scuseria, G. E.; Frisch, M. J. An Efficient Implementation of Time-Dependent Density-Functional Theory for the Calculation of Excitation Energies of Large Molecules. *J. Chem. Phys.* **1998**, *109*, 8218−8224.
(46) Furche, F.; Ahlrichs, R. Adiabatic Time-Dependent Density Functional Methods for Excited State Properties. *J. Chem. Phys.* **2002**, *117*, 7433−7447.
(47) Grimme, S. Semiempirical GGA-Type Density Functional Constructed With a Long-Range Dispersion Correction. *J. Comput. Chem.* **2006**, *27*, 1787−1799.
(48) Perdew, J. P.; Burke, K.; Ernzerhof, M. Generalized Gradient Approximation Made Simple. *Phys. Rev. Lett.* **1996**, *77*, 3865−3868.
(49) Perdew, J. P.; Burke, K.; Ernzerhof, M. Generalized Gradient Approximation Made Simple. *Phys. Rev. Lett.* **1997**, *78*, 1396−1396.
(50) Chai, J.-D.; Head-Gordon, M. Systematic Optimization of Long-Range Corrected Hybrid Density Functionals. *J. Chem. Phys.* **2008**, *128*, 084106.
(51) Zhao, Y.; Truhlar, D. G. The M06 Suite of Density Functionals for Main Group Thermochemistry, Thermochemical Kinetics, Noncovalent Interactions, Excited States, and Transition Elements: Two New Functionals and Systematic Testing of Four M06-Class Functionals and 12 Other Functionals. *Theor. Chem. Acc.* **2008**, *120*, 215−241.
(52) Yanai, T.; Tew, D. P.; Handy, N. C. A New Hybrid Exchange−Correlation Functional Using the Coulomb-Attenuating Method (CAM-B3LYP). *Chem. Phys. Lett.* **2004**, *393*, 51−57.
(53) Cossi, M.; Rega, N.; Scalmani, G.; Barone, V. Energies, Structures, and Electronic Properties of Molecules in Solution with the C-PCM Solvation Model. *J. Comput. Chem.* **2003**, *24*, 669−681.
(54) Hitachi High-Technologies GLOBAL. Analysis of 2,4-DNPH-Derivatized Aldehydes. https://www.hitachi-hightech.com/global/products/science/tech/ana/lc/chromaster/data16.html, accessed May 3, 2019.

DOI: 10.1021/acs.jpca.9b03588
J. Phys. Chem. A 2019, 123, 4863−4872